

## PRESTA: THE PARAMETER REDUCED ELECTRON-STEP TRANSPORT ALGORITHM FOR ELECTRON MONTE CARLO TRANSPORT

Alex F. BIELAJEW and D.W.O. ROGERS

*Ionizing Radiation Standards Section, Division of Physics, National Research Council of Canada, Ottawa, Ontario, Canada K1A 0R6*

Received 21 July 1986

A new electron transport algorithm for use with electron Monte Carlo transport codes is presented. Its components are: a path-length correction (PLC) algorithm which is based on the multiple scattering theory of Molière and which takes into account the differences between the straight path length and the total curved path length for each electron step; a lateral correlation algorithm (LCA) which takes into account lateral transport; and a boundary crossing algorithm (BCA) which ensures that electrons are transported accurately in the vicinity of interfaces. The algorithm has been implemented in the EGS4 code system and a variety of tests validating the algorithms are presented. In its standard configuration, use of this algorithm will allow the inexperienced user to obtain reliable results from the EGS Monte Carlo code without having to do a detailed study of the electron transport parameters. In many situations, substantial savings in computing time may be realized in comparison to the present EGS algorithm. The developments described in this report may be adapted to other electron transport codes where many of the same conclusions may be drawn.

### 1. Introduction

All electron Monte Carlo transport codes which accurately simulate electron transport demonstrate a strong dependence on electron step-size in the energy region up to 10 or 20 MeV [1–3]. Generally it is found that reducing the electron step-size causes the results to converge to the correct values while the computing time increases rapidly, in proportion to the inverse of the step-size. One is therefore faced either with a tedious study to determine the optimum step-size or with using a sufficiently small step-size to “be sure” of getting the correct results while using a great deal of computing time.

The purpose of this work was to reduce both the user’s time and the computing time required to do accurate electron transport calculations. One goal was to develop an electron transport algorithm which automatically selects the optimum step-size, thereby saving the user’s time. The second goal was to increase computing efficiency by developing techniques which allow larger step-sizes to be used accurately. We have developed a new Monte Carlo electron-transport algorithm called PRESTA, an acronym that stands for **Parameter Reduced Electron-Step Transport Algorithm**. The algorithm consists of several interrelated components.

The first of these is the incorporation of a path-length correction (PLC) algorithm that correctly accounts for the difference between the lengths of the electron’s curved path and its straight-line path. This curvature of

the electron’s path is due to elastic scattering from the nuclei and atomic electrons of the medium in which the transport takes place (see fig. 1). Some electron Monte Carlo codes do not include such a correction (e.g. ETRAN based codes or the codes of Nahum [2] or Andreo [4]). They overcome this shortcoming by using such small steps that there is little PLC required. Although EGS does incorporate a PLC algorithm, it is based upon the Fermi–Eyges multiple scattering theory [5] and this approach will be shown to be inadequate for accurate work. Rather, a new PLC based upon the Molière scattering theory [6,7] is presented. This provides a logical internal consistency for our implementation of the algorithm in the EGS code since the Molière theory is used for the selection of the multiple scattering

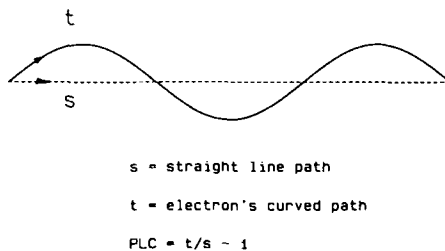


Fig. 1. The PLC (path-length correction) defined as  $t/s - 1$  accounts for the difference in length for each electron step between the electron’s total curved path  $t$ , and the straight-line path  $s$ , which is used in the transport model.

angle in EGS. However, the algorithm should enhance any electron Monte Carlo simulation. We show that the use of the Molière multiple scattering theory coupled to the new PLC is virtually independent of the step-size in the domain in which it is valid (no energy loss, transport in infinite, homogeneous media, step-sizes within the validity criteria of the Molière theory). In conjunction with the other elements in the PRESTA algorithm, we also show it is accurate in realistic calculations.

The second ingredient in the PRESTA algorithm is the incorporation of a lateral correlation algorithm (LCA) that performs a translation perpendicular to the direction of motion during an electron transport step (see fig. 2). This becomes essential because the new PLC algorithm allows such large electron steps that this lateral displacement becomes significant. Tests of the LCA under idealized conditions show that artefacts associated with step-size dependence of lateral transport are nearly eliminated.

The final ingredient required for the PRESTA algorithm is an efficient and reliable method for treating the electron transport near the interface between regions. This requirement has been recognized before [8] but we expand on this original theme. We present a general solution for our implementation in the EGS4 system in which electrons are forced to stop at boundaries. However, the concepts involved could be applied to other codes which can have different algorithms for changing media. Fig. 3 shows an electron step taking place in one medium adjacent to another.

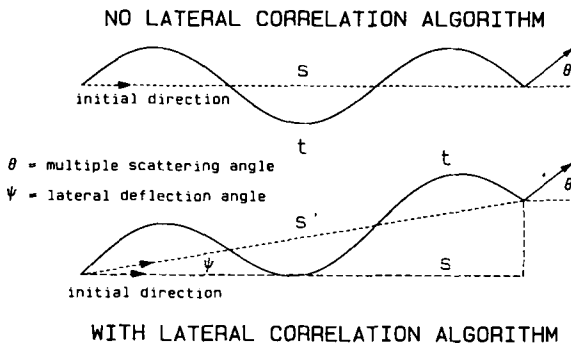


Fig. 2. When no lateral displacements are taken into account (upper trajectory) the curved step  $t$  is considered to end at the same point as the straight step in the original direction of motion. In EGS the multiple scattering angle  $\theta$  is applied at the end of the step. If lateral displacements are taken into account (lower trajectory), there is a lateral deflection angle  $\psi$  which is applied at the beginning of the step. The multiple scattering angle  $\theta$  is still applied with respect to the initial direction. The PLC is still defined in terms of the original straight-line path-length  $s$  and thus  $s'$ , the actual straight-line path-length traversed, is increased when lateral displacements are included.

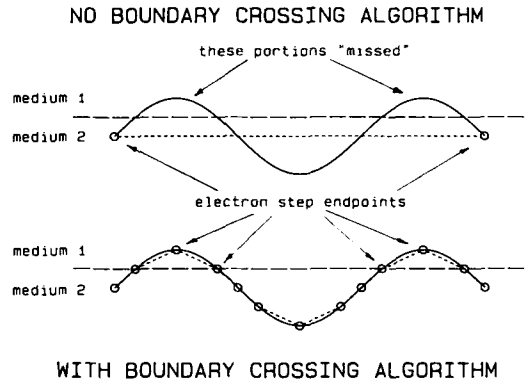


Fig. 3. In current algorithms, if a long step is taken near a boundary, the algorithm erroneously treats the step as occurring entirely on one side of the boundary whereas a certain subset of the electrons being simulated would actually cross the boundary. In many situations this causes no significant problems but in some it is critical. To solve the problem in general requires taking short steps near the boundary.

All condensed history electron transport algorithms move the electrons in a straight line for each step. Whether or not the codes take it into account, the electron's path is actually curved. For very short steps the difference between the straight path and the curved path is negligible, but for large steps it can be significant. Part of this curved path may take place in the other region. However, current algorithms must assume that all of the curved path takes place in the region containing the endpoints of the straight-line path. As indicated, the solution is to shorten the electron path in the vicinity of the interface and actually track into the other region that subset of electron histories which would have gone there. We describe in detail how this "boundary crossing algorithm" can be incorporated in a transport code.

Far away from boundaries the simulation of large electron steps becomes possible, and the PRESTA algorithm must accurately account for energy loss during the course of this long step. We demonstrate that the inclusion of energy loss introduces no new step-size dependence as long as the energy is taken to be that at the mid-point of the step.

Finally, we apply PRESTA to some realistic problems that highlight the development of the various components. We compare these results to those obtained using other, simpler electron transport algorithms and contrast the amount of computing time used by the various methods.

In the final section we summarize our results and indicate which areas need attention for further improvement. In this report we present only an overview of our results. The detailed derivations and notes on implementation in EGS4 are given in an internal report [9].

## 2. A new path-length correction theory

In this section we propose a new PLC theory, discuss its limitations and demonstrate the step-size independence of this theory under idealized conditions.

### 2.1. The Molière theory

First, we establish a notation which is consistent with that found in the EGS manuals [10,11]. We start with the following set of parameters of the Molière theory:

$$\Omega_0 = b_c t / \beta^2, \quad (2.1)$$

$$\chi_c^2 = \chi_{cc}^2 t / E^2 \beta^4, \quad (2.2)$$

where  $b_c$  and  $\chi_{cc}$  are constants that depend only on the medium in which the transport takes place \*,  $\beta$  is the ratio of the magnitude of the electron's velocity in units of the speed of light,  $E$  is the total energy (kinetic plus rest mass) of the electron and  $t$  is the total curved path-length of the electron step.  $\Omega_0$  can be interpreted as the number of atomic collisions that contribute to the scattering and Molière considered his theory valid for  $\Omega_0 > 20$ .

The Molière multiple scattering angle distribution is given by:

$$f(\theta) \theta d\theta = f_r(\phi) \phi d\phi, \quad (2.3)$$

where  $\theta$ , the scattering angle, and  $\phi$ , the "reduced" angle are related by

$$\phi = \theta / \chi_c B^{1/2}, \quad (2.4)$$

where

$$B - \ln B = b = \ln \Omega_0, \quad (2.5)$$

defines both  $B$  and  $b$ . From eq. (2.5) we see that we must restrict  $\Omega_0 > e$  or else  $B$  is a double-valued function of  $b$ . The Molière distribution can be expanded in a power series in  $1/B$ ,

$$f_r(\phi) = f^{(0)}(\phi) + \frac{f^{(1)}(\phi)}{B} + \frac{f^{(2)}(\phi)}{B^2} + \dots, \quad (2.6)$$

where

$$f^{(0)}(\phi) = 2e^{-\phi^2} \quad (2.7)$$

and  $f^{(1)}$  and  $f^{(2)}$  are given in numerical form by Bethe

\* For monoatomic substances

$$b_c = 6702.33 \rho \frac{Z^{1/3}(Z+1)}{M} \frac{1}{1+0.000178Z^2} \text{ (cm}^{-1}\text{)},$$

$$\chi_{cc} = 0.39612 \sqrt{\frac{Z(Z+1)\rho}{M}} \text{ (MeV cm}^{-1/2}\text{)},$$

where  $\rho$  = density in  $\text{g cm}^{-3}$ ,  $Z$  = atomic number,  $M$  = atomic weight in  $\text{g/mole}$ . For polyatomic substances, similar expressions are given by Nelson et al. [11].

(1953). The expansion expressed by eq. (2.6) is strictly valid only for  $B > 1$  ( $\Omega_0 > e$ ) since the  $f^{(n)}$ 's are of the order unity or less. This restriction imposes an absolute lower limit on the step-size, somewhat smaller than that proposed by Molière's  $\Omega_0 > 20$  ( $B > 4.5$ ). Using the smaller criterion, we see from eq. (2.1) that the minimum step-size is given by

$$t_{\min} = e\beta^2/b_c. \quad (2.8)$$

$\rho t_{\min}/\beta^2$  is approximately  $4 \times 10^{-4} \text{ g cm}^{-2}$  for  $\text{H}_2\text{O}$  ( $\rho$  is the density). For other materials the relative dependence is approximately governed by a  $1/Z$  factor, where  $Z$  is the average atomic number. This is an exceedingly small number for many practical purposes (see fig. 4).

An upper limit on the electron step-length has been derived by Bethe [12] in his classic treatment of the Molière theory. Bethe has shown that the Molière theory, initially constructed as a small angle theory, and the theory of Goudsmit and Saunderson [13], which does not rely on a small angle approximation, are nearly equivalent as long as the following condition is satisfied:

$$\chi_c^2(t) B(t) \leq 1. \quad (2.9)$$

The quantity  $\chi_c^2 B$  is interpreted approximately as the mean-square scattering angle. Using eq. (2.9) along with eqs. (2.1), (2.2) and (2.5) allows us, after some manipulation, to write an equation for the maximum step-length,  $t_{\max}$ ,

$$t_{\max} = \frac{E^2 \beta^4}{\chi_{cc}^2 \ln(b_c E^2 \beta^2 / \chi_{cc}^2)}. \quad (2.10)$$

$t_{\max}$  and  $t_{\min}$  are plotted in fig. 4 for water. We note that  $t_{\max}$  and  $t_{\min}$  become equal for an energy of about

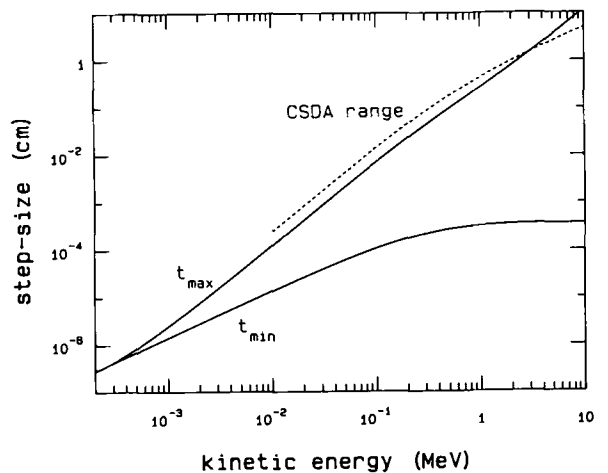


Fig. 4. The maximum (Bethe limit) and minimum ( $\Omega_0 \geq e$ ) step-size criteria for the Molière theory in water. Minimum and maximum step-sizes converge at about 230 eV in this case. The CSDA range (dashed line) is also shown. It becomes more restrictive than  $t_{\max}$  at about 3 MeV in water.

230 eV. This number can be derived by equating eqs. (2.8) and (2.10) and solving for the energy. The result is that the lowest kinetic energy allowed by the Molière theory is approximately

$$E_{k,\min} = \frac{eX_{cc}^2}{2b_c(m_0c^2)}, \quad (2.11)$$

where  $(m_0c^2)$  is the rest mass energy of the electron.  $E_{k,\min}$  is almost independent of material. It must be recognized that  $E_{k,\min}$  is an underestimate since low energy atomic processes are not fully modelled either by the Molière theory or by current condensed history Monte Carlo codes. The upper limit  $t_{\max}$  varies in the same fashion as  $t_{\min}$  for different materials, roughly by a relative  $1/\bar{Z}$  factor. Fig. 4 also shows the CSDA range [14] in water. The Molière theory does not include energy loss and the CSDA range was plotted to show an upper limit on where energy-loss physics would be expected to provide the more restrictive upper bound. For water this occurs at about 3 MeV.

The value of  $t_{\min}$  for water is plotted versus electron kinetic energy in fig. 5 where the step-size for various values of  $E_{\text{step}e}$  are also shown. ( $E_{\text{step}e}$  is the maximum fractional energy loss per electron step due to continuous processes. It is discussed in detail by Rogers [3]). This plot can be interpreted as follows: if one tries to use too low a value of  $E_{\text{step}e}$  one may enter the region where the lower limit of the Molière theory is violated. We do not know exactly how other codes handle very short steps, however, for step sizes below  $t_{\min}$ , no multiple scattering is performed with EGS, for lack of a

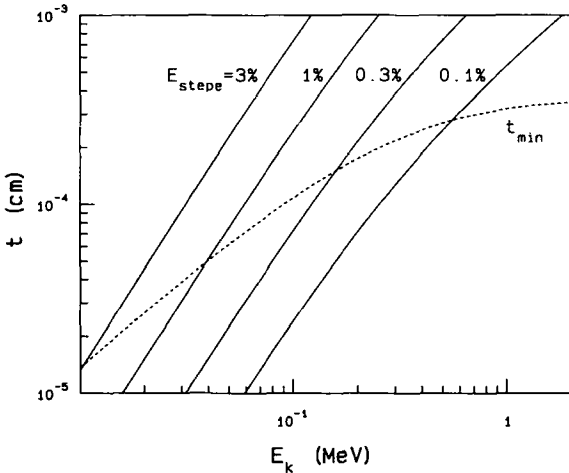


Fig. 5. Total step-size in water,  $t$ , as a function of electron kinetic energy for various values of  $E_{\text{step}e}$ , the maximum fractional energy loss per electron step due to continuous processes. Also shown is the value of the minimum step size for which multiple scattering theory holds,  $t_{\min}$ , as a function of energy (so for example, no multiple scattering would be done at energies below about 500 keV for  $E_{\text{step}e} = 0.1\%$ ).

theory to describe it. The default EGS value for  $t_{\min}$  is chosen to be  $\Omega_0 = 1$ , not  $e$  as in the present case. An extrapolation is performed below  $\Omega_0 = e$  in the default EGS version to relate  $B$  and  $\Omega_0$  since eq. (2.5) is only valid above  $\Omega_0 = e$ . This “turning off multiple scattering” can lead to remarkable artefacts in calculated results where step-size restrictions below  $t_{\min}$  are imposed [3,8]. The PRESTA algorithm does not allow a user to violate the minimum step-size limit by choosing too low a value for  $E_{\text{step}e}$ .

## 2.2. The basic path-length correction theory

In the development of the new PLC theory that follows, we use only the first two terms in the Molière expansion of eq. (2.6) and we work to order  $1/B$ . Bethe [12] has discussed the consequences of neglecting the second order term and we have found that the inclusion of the  $f^{(2)}$  and  $1/B^2$  terms offers no improvement to the PLC. For the sake of simplicity, we leave them out.

The total curved path of an electron step,  $t$ , and the average straight-line distance of the step in the direction of motion at the beginning of the step,  $s$  (see figs. 1,2), are related by the following equation, attributed to Lewis [15]:

$$s = \int_0^t dt' \langle \cos \theta(t') \rangle, \quad (2.12)$$

where the average value,  $\langle \rangle$ , denotes an average computed with any multiple scattering theory. Berger [16] has proposed the following approximation to eq. (2.12),

$$s = \frac{1}{2}t(1 + \cos \theta(t)), \quad (2.13)$$

where the multiple scattering angle is that which is selected from the multiple scattering distribution for the electron step. We have verified that eq. (2.13), when  $\theta$  is selected from the Molière distribution, provides on average, excellent results in addition to faster computational speed per step compared to the PLC we present below. Yet, we do not use this method for several reasons. First, for a given  $t$  eq. (2.13) produces a straggling distribution of  $s$  values about its correct mean value. This straggling component appears to be overestimated. Secondly, this straggling leads to increased variation of quantities dependent on the PLC. This offsets the advantage of computational speed per step. For these reasons we have constructed a PLC using eq. (2.12).

Equation (2.12) is difficult to use directly with the Molière distribution and we have found that an expansion to 4th order in  $\theta$  is adequate. Therefore, we approximate

$$s = t - \frac{1}{2} \int_0^t dt' \langle \theta^2(t') \rangle + \frac{1}{24} \int_0^t dt' \langle \theta^4(t') \rangle. \quad (2.14)$$

This expression up to second order in  $\theta$  has been proposed by Yang [17] and we have found that the

inclusion of the  $\theta^4$  term offers a small but noticeable improvement. Since this correction is small and the Molière distribution is dominated by the  $f^{(0)}$  term, we do not include the  $f^{(1)}$  term in the  $\theta^4$  integral.

In Bethe's treatment of the Molière theory [12], he derived a correction of the form  $(\sin\theta/\theta)^{1/2}$  that should multiply the Molière distribution to correct it for large-angle scattering. By expanding this factor to order  $\theta^4$  and substituting the Molière expansion function as described we obtain

$$t = s + \frac{1}{2} \int_0^\pi dt' \chi_c^2 B \left\{ \left( 1 - \frac{1}{4} \chi_c^2 B \right) + \frac{1}{2B} \int_0^{\pi^2/\chi_c^2 B} dx \left[ (x-1) - \frac{1}{12} (\chi_c^2 B) x(x-2) \right] \times f^{(1)}(x) \right\}, \quad (2.15)$$

where the following relations were used:

$$\int_0^\infty d\theta \theta^{2n+1} f^{(0)}(\theta) = n! (\chi_c^2 B)^{n+1}, \quad (2.16)$$

$$\int_0^\pi d\theta \theta^{2n+1} f^{(1)}(\theta) = \frac{1}{2} (\chi_c^2 B)^{n+1} \int_0^{\pi^2/\chi_c^2 B} dx x^n f^{(1)}(x), \quad (2.17)$$

$$x \equiv \phi^2. \quad (2.18)$$

In eq. (2.16) we may integrate beyond the maximum physical angle,  $\theta = \pi$ , with very little error. The result follows directly from the substitution of the Gaussian term in eq. (2.7). In eq. (2.17), however, we must terminate the integration at  $\theta = \pi$  or else the asymptotic Rutherford scattering form of  $f^{(1)}$ ,

$$f^{(1)} \phi \xrightarrow{\phi \rightarrow \infty} \frac{2}{\phi^4}. \quad (2.19)$$

produces spurious infinities that result from the small-angle approximation in the analysis.

Finally, as stated previously, the Molière theory is not well-defined for  $t < t_{\min}$ . Therefore, for  $t > t_{\min}$ , we approximate

$$t = s + \frac{\chi_{cc}^2}{4E^2\beta^4} t_{\min}^2 + \frac{1}{2} \int_{t_{\min}}^t dt' \chi_c^2 B \left\{ \left( 1 - \frac{1}{4} \chi_c^2 B \right) + \frac{1}{2B} \int_0^{\pi^2/\chi_c^2 B} dx \left[ (x-1) - \frac{1}{12} (\chi_c^2 B) x(x-2) \right] \times f^{(1)}(x) \right\} \quad (2.20a)$$

and for  $t \leq t_{\min}$ ,

$$t = s. \quad (2.20b)$$

The extra term in eq. (2.20a) can be derived by assuming that the correction comes entirely from the  $f^{(0)}$  term with  $B$  set equal to unity for  $t < t_{\min}$ . While the inclusion of this term is not particularly well motivated

physically it was found to improve the consistency of the PLC at low energies and small step sizes.

Eq. (2.20) constitutes the new PLC theory. Given a value of  $t$ ,  $s$  is predicted directly. While it is not intrinsically complicated, the recasting of this equation into a form suitable for rapid calculation involves much detail and is left for an internal report [9].

### 2.3. Results of the new PLC under idealized conditions

In fig. 6 we have plotted the new PLC, i.e.  $(t/s - 1)$ , in water versus the electron kinetic energy,  $E_k$  for various step-sizes as determined by the expression  $t = E_{\text{step}} E_k / S_{\text{col}}(E_k)$ , where the unrestricted collision stopping power,  $S_{\text{col}}$ , has been obtained from Berger and Seltzer [14] and  $E_{\text{step}}$  is the fractional electron energy loss per step due to collision processes. These results do not include the effect of energy loss in the step although the final PRESTA algorithm takes this into account. We have also shown the PLC for the maximum step-size,  $t_{\max}$ , which is almost constant at about 0.28. Again, we see that the range (here shown as the 100% curve, i.e. approximated by  $E_k/S_{\text{col}}$ ) becomes more restrictive above about 3 MeV. Below this energy,  $t_{\max}$  becomes the more restrictive upper bound. However, energy losses of at least 28% are allowed at low energies. The "leveling off" of the PLC at low energies reflects the fact that the stopping power is increasing for lower energy roughly in proportion to the increased PLC.

A fair and unambiguous test of the stability of the

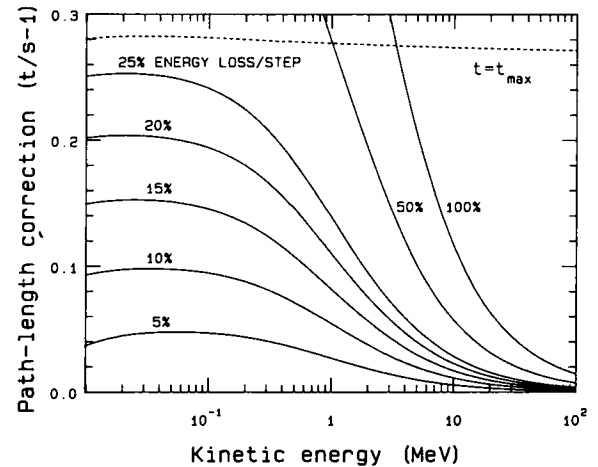


Fig. 6. The PLC versus electron kinetic energy for various fractional energy losses per electron step in water. Also shown is the PLC for step-sizes corresponding to  $t_{\max}$  (eq. 2.10). The  $t_{\max}$  restriction allows an energy loss of up to 28% for low energies increasing to 100% for energies above 3 MeV. For low energies the PLC is approximately equal to the fractional energy loss. These results do not include the energy loss corrections (discussed in section 4).

Molière theory and the new PLC can be done by “turning off” any of the physical processes which might obscure the interpretation. To this end we turn off, for the moment, all continuous and discrete energy loss processes and consider transport in an infinite, homogeneous medium (water for the present consideration). Here, and elsewhere, we use the EGS4 code system for our calculations although the tests are designed to examine the various new algorithms rather than the original system. We start the particle off in a certain direction (which we call the  $z$ -direction) and allow a transport step equal in step-size to  $t_{\max}$  to occur and calculate the average straight-line distance in the original direction of motion,  $\langle z \rangle_1$ . We then repeat this study for two steps of size  $t_{\max}/2$ , three steps of size  $t_{\max}/3$ , etc. We note that for the single step,  $s(t_{\max}) = \langle z \rangle_1$  is calculated analytically from eq. (2.20) and does not depend on the selection of the multiple scattering angle

which, in EGS, is determined at the end of the step (consult fig. 1). For the other fractions

$$\langle z \rangle_N = s(t_{\max}/N) \left( 1 + \sum_{n=1}^{N-1} \cos \theta_{z,n} \right) \quad (2.21)$$

where  $\theta_{z,n}$  is the angle made with the  $z$ -axis after the  $n$ th step and  $N$  is the total number of steps.  $\theta_{z,n}$  can be related to the multiple scattering angle of the previous step. These multiple scattering angles are selected from the Molière distributions and consequently  $\langle z \rangle_N$  depends both on the PLC and the Molière scattering angle for  $N > 1$ . *If the PLC and the Molière theory are both physically consistent, then  $\langle z \rangle_N$  should be independent of  $N$ , or equivalently, step-size independent.*

In fig. 7 we demonstrate the stability of  $\langle z \rangle_N$  in water for 10 MeV, 1 MeV, 100 keV and 10 keV electrons. We also demonstrate the effect of turning off the PLC (setting  $t = s$  for each step) and we also show the

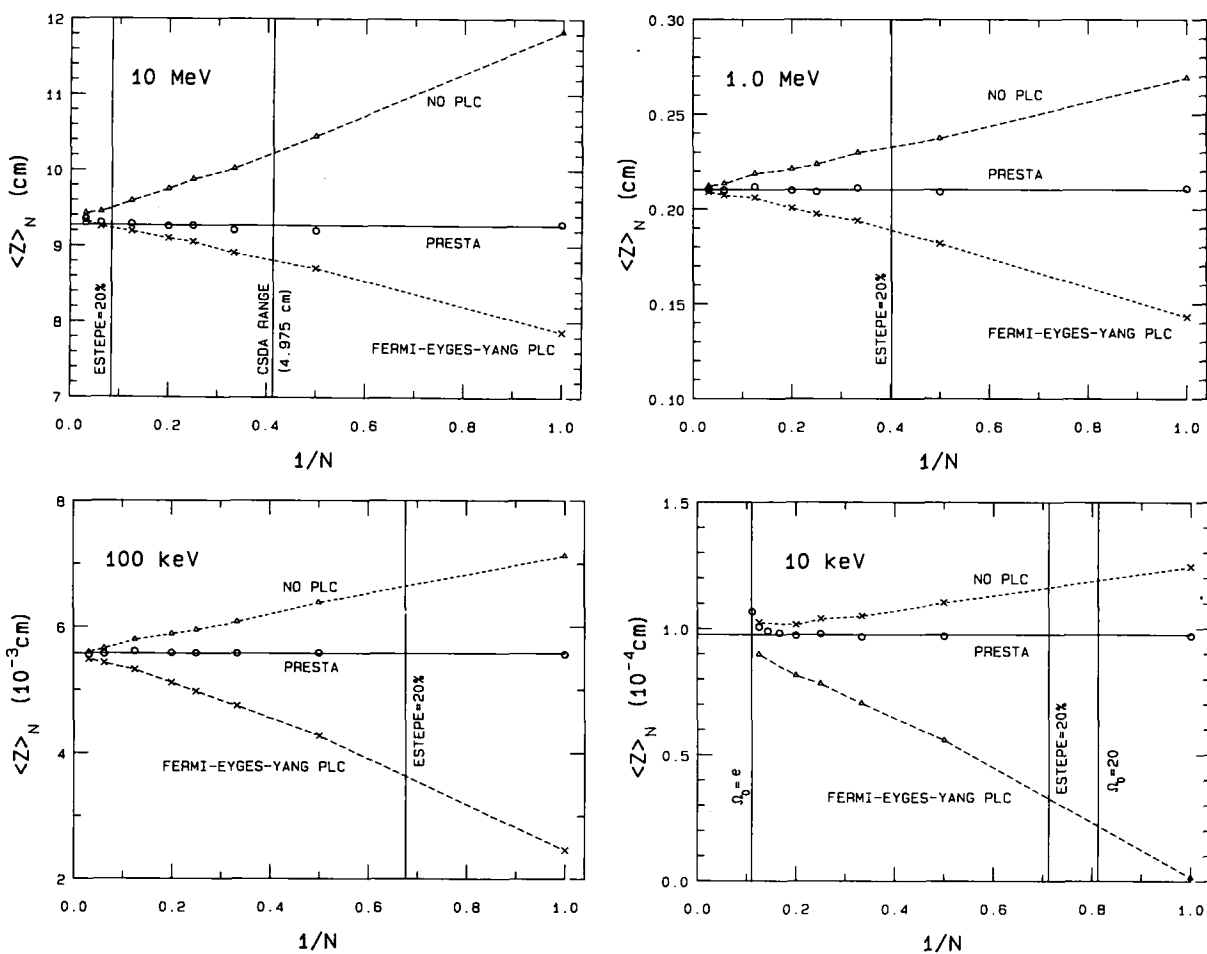


Fig. 7. A test of the PLC algorithm vs other algorithms. The average straight-line distance in water in the original direction of motion after a total curved path-length of  $t_{\max}$ , as a function of  $1/N$ , the inverse of the number of steps taken. Energy loss is not included in the calculations. The values of  $N$  that would give individual curved path-lengths equal to the CSDA range and/or a 20%  $E_{\text{step}}$  are shown, as are the corresponding values for steps producing  $\Omega_0 = e$  and 20 for the 10 keV case.

results using the Fermi–Eyges–Yang PLC, the standard PLC in EGS. The new PLC (labelled PRESTA) shows excellent step-size stability. The NO PLC cases exhibit large overestimates which could have been anticipated from the magnitude of the PLC depicted in fig. 6. The Fermi–Eyges–Yang PLC appears to underestimate by approximately the same amount. Thus, the Fermi–Eyges–Yang theory calculates too much PLC for a given step-size. In every case, however, all these methods converge to the same values for the smaller step-sizes since the path-length correction tends to zero for small step-sizes.

Some specific comments need to be made, however. In the 10 MeV case, we show the value of  $N$  corresponding to steps equal to the CSDA range [14]. Thus, the larger step-sizes would exceed this range if energy loss were incorporated. Keeping this in mind, we conclude that PLC's becomes less important at higher energies as is also demonstrated by figure 6. However, at 10 MeV the correction still can be of the order of 10% for very large steps with the Fermi–Eyges–Yang PLC performing somewhat better than the NO PLC case. At lower energies the NO PLC cases exhibit some improvement over the Fermi–Eyges–Yang PLC but the discrepancies are still substantial for large step-sizes. These figures are plotted in terms of steps which are a fraction of  $t_{\max}$ , the relevant parameter in the context of the theory. However, to tie this to the more commonly used concept of fractional energy loss per step, we have indicated on each graph the value of  $1/N$  which would produce a 20% energy loss in each electron step (if energy loss were included). For the 10 keV case we have also indicated the step-size corresponding to Molière's lower limit criterion,  $\Omega_0 = 20$ , as well as the mathematical limit,  $\Omega_0 = e$ , described earlier. It appears that the Molière lower limit is somewhat too conservative and we shall assume that the lower mathematical limit is acceptable. There is some evidence that the new PLC is breaking down slightly near this lower limit.

We have also studied the stability of the PLC for other materials and observe no degradation for high or low- $Z$  materials.

### 3. The lateral correlation algorithm

As discussed in the introduction, most electron Monte Carlo codes do not account for lateral transport during the course of a transport step (see fig. 2). However, by breaking the transport history into small steps and deflecting the particle at the end of each transport step, one effectively accomplishes the lateral transport of an electron. Most codes must use small steps to overcome the lack of path-length corrections and hence the lack of lateral transport during a step has not been a problem. Since we can use large electron steps with the

new PLC, it is necessary to include a method that accounts for the lateral deflection during the course of each step if we wish to obtain step-size independence of physical results that may depend on lateral transport.

Berger [16] has proposed a method to account for this lateral transport. Neglecting his straggling term which provides fluctuations about mean values, we write the deflections along the two orthogonal directions perpendicular to the original direction, as

$$x = \frac{1}{2}t \sin \theta \cos \alpha, \quad (3.1a)$$

$$y = \frac{1}{2}t \sin \theta \sin \alpha, \quad (3.1b)$$

where we have assumed an initial position at the origin and an initial direction along the  $z$ -axis and  $\alpha$  is an azimuthal angle selected randomly over the range  $0 \leq \alpha < 2\pi$ . However,  $x$  and  $y$  are distributed quantities and this follows from their direct connection to the multiple scattering angle,  $\theta$ .

It should be noted that eq. (3.1) cannot be derived directly from the Fermi–Eyges [5] multiple scattering theory. Rather, one can derive, in the limit of small deflections and small energy losses, that  $x = \frac{1}{2}s\theta \cos \alpha$ ,  $y = \frac{1}{2}s\theta \sin \alpha$ . One makes the extrapolation to large angles by replacing  $s$  by  $t$  and  $\theta$  by  $\sin \theta$ . Physically, this argument is sound because  $t$ , not  $s$ , is the effective thickness of material the electron travels through and  $\sin \theta$  rather than  $\theta$  obeys the intuitive expectation of reaching a maximum at  $\pi/2$  and a minimum at  $\pi$ . Although a straggling term is necessary to describe the physics completely, we have not adopted the one proposed by Berger [16]. Its inclusion appeared to have a deleterious effect on the tests we have applied to it. We can only speculate on the reasons for this. However, there is a need for further research in this area. We call eq. (3.1) the lateral correlation algorithm (LCA) because the size of the lateral deflection is correlated with the multiple scattering angle,  $\theta$ . Additionally, we set the upper limit  $\sqrt{t^2 - s^2}$  on the lateral deflection  $\sqrt{x^2 + y^2}$ . This prevents the unphysical circumstance of having  $s$ , the straight-line distance between the electron step endpoints, exceed  $t$ , the total curved path. As discussed below, we do not invoke the LCA whenever a particle is closer than the total curved path-length  $t$  from any boundary since otherwise the LCA could cause the particle to cross the boundary and it would be computationally expensive to check for this at every step.

Again, to test eq. (3.1) fairly and unambiguously we turn off all energy-loss mechanisms and consider electron transport in an infinite, unbounded medium. Initially, we allow a transport step of size  $t_{\max}$  to occur and we use eq. (3.1) to specify the lateral correlation. We then determine the average perpendicular direction,  $\langle r \rangle_1$ , from the line along the original direction of motion. Then, we repeat the calculation for two steps of size  $t_{\max}/2$ , three steps of size  $t_{\max}/3$ , etc. Again, if the multiple scattering distribution and the LCA are physi-

in the Introduction, if the steps adjacent to a boundary are too large, then various types of artefacts can occur. We have seen in fig. 3 an example of how the current EGS algorithm treats an electron step near a boundary. Most Monte Carlo codes allow long steps adjacent to a boundary between two regions when part of the total curved path can actually take place physically in the region across the boundary. Nonetheless they treat the transport step as if it occurred entirely in the region that contains the endpoints of the step, neglecting the contribution to adjacent regions. This can lead to severe problems, especially if there is a significant material or density change at the boundary.

To circumvent this problem, one must shorten the electron steps in the vicinity of an interface to ensure that electrons which may cross the boundary actually have an opportunity to do so. To this end, we limit the total curved path of the transport step to the minimum of  $t_{\max}$  and  $t_{\text{perp}}$ , where  $t_{\text{perp}}$  is the smallest perpendicular distance to any boundary and  $t_{\max}$  is given by eq. (2.10). For steps of this kind, since no part of the total curved path can take place in any other region, the electron can be considered to be in an infinite medium. We can only allow this truncation to occur so far, otherwise the electron would never cross the boundary unless it was coming at it exactly normally. This truncation is not allowed to reduce the step below  $t'_{\min}$  where

$$t'_{\min} = f_{\min} t_{\min}. \quad (5.1)$$

The quantity  $f_{\min}$  is a number greater than or equal to unity and  $t_{\min}$  is given by eq. (2.8). For maximum efficiency we equate  $t'_{\min}$  to  $t_{\max}$  for the lowest energy electron that can be transported as defined by the parameter  $E_{\text{cut}}$ , which includes the rest mass [10,11]. Using eqs. (5.1), (2.8) and (2.10) we may solve for  $f_{\min}$  and obtain

$$f_{\min} = \frac{b_c (E_{\text{cut}}^2 - (m_0 c^2)^2)}{e \chi_{\text{cc}}^2 \ln \left( b_c (E_{\text{cut}}^2 - (m_0 c^2)^2) / \chi_{\text{cc}}^2 \right)}. \quad (5.2)$$

From eqs. (2.1) and (2.5) we see that we may define

$$b_{\min} = 1 + \ln f_{\min} = \ln \left[ \frac{b_c (E_{\text{cut}}^2 - (m_0 c^2)^2)}{\left( \chi_{\text{cc}}^2 \ln \left( b_c (E_{\text{cut}}^2 - (m_0 c^2)^2) / \chi_{\text{cc}}^2 \right) \right)} \right]. \quad (5.3)$$

For  $E_{\text{cut}}$  values corresponding to kinetic energies of 1 keV, 10 keV, 100 keV and 1 MeV in water  $b_{\min}$  is 1.56, 3.20, 5.18 and 7.74, respectively. For an electron in water with 1 MeV kinetic energy, these correspond to minimum steps corresponding to energy losses of about 0.070, 0.43, 3.5 and 50% respectively.

For steps which would otherwise be greater than  $t_{\text{perp}}$  when  $t_{\text{perp}}$  is less than  $t'_{\min}$ , the curved path is reduced if necessary to  $t'_{\min}$  instead of  $t_{\text{perp}}$ . The PRE-

STA routine, as implemented in EGS, then checks with the geometry routine HOWFAR [10,11] to see if the trajectory of the electron would allow it to cross the boundary. In this case, if the trajectory allows for it, the electron step is shortened placing it on the boundary. For any step with the step length greater than  $t_{\text{perp}}$  (whether or not it actually intercepts the boundary), the LCA is not invoked to prevent any ambiguity as to which region contains the endpoint of the step. This should not cause any problems because the step is already short.

This boundary crossing algorithm (BCA) is invoked both for particles approaching and drawing away from a boundary. PRESTA uses the BCA with  $b_{\min}$  as defined by eq. (5.3). This algorithm makes great demands on computing time if there are many boundaries in the problem or if  $E_{\text{cut}}$  is very low. An experienced user may decide to alter  $b_{\min}$  or turn off the BCA in certain circumstances. These options are available to the user and are described in the implementation notes [9].

We remark that the default for the minimum step-size is now a strong function of  $E_{\text{cut}}$ , and this can introduce an  $E_{\text{cut}}$  dependence which does not occur in normal EGS calculations. This is because  $E_{\text{cut}}$  now helps define how boundaries are approached (via eq. (5.2)). However, if the user chooses an  $E_{\text{cut}}$  that is low enough for accurate electron transport in a given application, then the default minimum step-size will usually ensure that the approach and withdrawal from boundaries is slow enough to ameliorate boundary-associated artefacts for all electrons in the simulation. If too large a value of  $E_{\text{cut}}$  is used in comparison to the electron energy of interest in the problem, then all electrons may take steps that are too large in the vicinity of interfaces. Moreover, one risks the deleterious effect of having a large fraction of all electron steps terminate on boundaries. As discussed above, the LCA is not invoked under these circumstances. Thus, if lateral transport is important, inaccuracies may be introduced. Under most circumstances, the proper choice of  $E_{\text{cut}}$  should remedy this problem. In other circumstances it may be desirable to retain a relatively high value of  $E_{\text{cut}}$  and still require accurate electron transport. To avoid inaccuracies as described above the user may choose to reduce the minimum step-size by lowering  $b_{\min}$  as described in the implementation notes [9].

In such situations where the geometrical constraints may cause difficulty in the choice of  $E_{\text{cut}}$  or  $b_{\min}$ , one should compare, for the maximum energy of interest in the problem, the value of  $t'_{\min}$  from eq. (5.1) or the equivalent expression,

$$t'_{\min} = \beta^2 e^{b_{\min}} / b_c \quad (5.4)$$

with the minimum relevant characteristic dimension in the problem (for example, the slab thickness in a depth-dose calculation) and guarantee that  $t'_{\min}$  is only

a fraction of it by either lowering  $E_{\text{cut}}$  or overriding the  $b_{\text{min}}$  default value. Alternatively, one may place a further constraint on the step-size by insisting that no charged particle step exceed a certain distance. (This quantity is called SMAX in EGS and is fully described by Rogers [3]).

## 6. PRESTA

Putting all the above components together gives the PRESTA algorithm which can be summarized as follows.

For each electron step, the difference between the total curved path length and the straight line path length is accounted for using a new path-length correction (PLC) algorithm which is given by eq. (2.20). This algorithm has been shown to be accurate for steps greater than  $t_{\text{min}}$  (given by eq. (2.8)) and less than  $t_{\text{max}}$  (eq. (2.10)). These values define the limits of applicability of the underlying Molière multiple scattering theory. For the occasional steps taken with  $t < t_{\text{min}}$  (near boundaries or before discrete events), neither multiple scattering nor PLC is done.

With an accurate PLC available, it is possible to take much larger steps than was previously possible, except that three other aspects of the problem must be taken into account.

Firstly, in the PLC and other algorithms, it becomes essential to evaluate all quantities at the energy midpoint of the step.

Secondly, for accurate simulations in the vicinity of an interface, one must take care that no part of the actual curved path of the electron being transported on one side of the interface can take place in the region across the interface. For this reason, as we approach and leave a boundary or do any transport near a boundary, PRESTA limits steps to  $t \leq t_{\text{perp}}$ , where  $t_{\text{perp}}$  is the closest distance to any boundary (not necessarily along the path of the electron). To allow electrons to cross a boundary, this algorithm is not allowed to reduce the step size below  $t'_{\text{min}}$  as given by eqs. (5.1) and (5.2). Note that  $t'_{\text{min}}$  is chosen automatically and is a function of the input parameter  $E_{\text{cut}}$ . Only under special circumstances described in section 5 will the user find it necessary to lower the value of  $t'_{\text{min}}$ .

Finally, for large steps the lateral deflection of each individual step becomes significant and this is incorporated using the lateral correlation algorithm (LCA) defined in eq. (3.1) along with a maximum value of  $\sqrt{t^2 - s^2}$ . Note that implementation of this LCA requires use of the boundary crossing algorithm to ensure that the particle is not moved out of its current region by the lateral movement. For those steps so close to a boundary that  $t < t'_{\text{min}}$ , the LCA is not invoked to prevent uncertainties as to what region the step ends in.

Note that the LCA increases the straight-line distance travelled by the electron for a given total path-length  $t$  since the PLC is defined in terms of the straight line path-length in the original direction and not the straight-line path-length after the LCA is used (see fig. 2).

These four elements define the electron transport algorithm, PRESTA.

## 7. Applications

In this section we apply PRESTA to some practical problems highlighting its strengths as well as its weaknesses.

### 7.1. Energy deposition at depth

Energy deposition at large depths in thick slabs is a good test for all the components of PRESTA. Therefore, we have simulated electron transport in a slab of water infinite in height and depth with one boundary situated at one-half the CSDA range,  $r_0$ , of the incident electron. A broad beam of electrons was incident normally on the face of the slab and the energy deposited beyond the boundary at  $\frac{1}{2}r_0$  was calculated. The creation of secondary particles was not done explicitly but was included implicitly by the use of total stopping powers. The energy at which the electron history was terminated was 1% of the incident energy except in the 10 keV case where 10% was used.

The results for 10 MeV, 1 MeV, 100 keV and 10 keV electrons in water are shown in fig. 11. The fractional energy deposited past  $r_0/2$  versus  $E_{\text{step}}$ , the maximum fractional energy loss per step, is depicted. In all cases, the points plotted at  $E_{\text{step}} = 0.2$  correspond to the default values,  $t = t_{\text{max}}$  for PRESTA, and  $t = 0.8t_{\text{max}}$  for NO PLC and the Fermi-Eyges-Yang PLC. (This 0.8 factor is the default for EGS.) For these latter two cases, the LCA and BCA were not invoked. PRESTA shows excellent stability over the range of step-sizes shown. Only for the 10 keV case do we see evidence of breakdown at the smaller step-sizes. The Fermi-Eyges-Yang PLC performs quite well at 10 MeV. In all cases, the simpler algorithms converge at small step-sizes to the PRESTA result.

It is instructive to consider the effects of turning off the BCA and LCA within PRESTA. In the 1 MeV case with the default  $E_{\text{step}}$ , turning off the LCA reduces the energy deposited past  $r_0/2$  by 4.5% and also turning off the BCA reduces the energy deposited by a further 6.7%. Turning off the BCA means that portions of the electron's path which would have gone past  $r_0/2$  due to the curvature of the electron step have not been properly accounted for, and hence the energy deposition at depth is reduced. The effect of the LCA is more com-

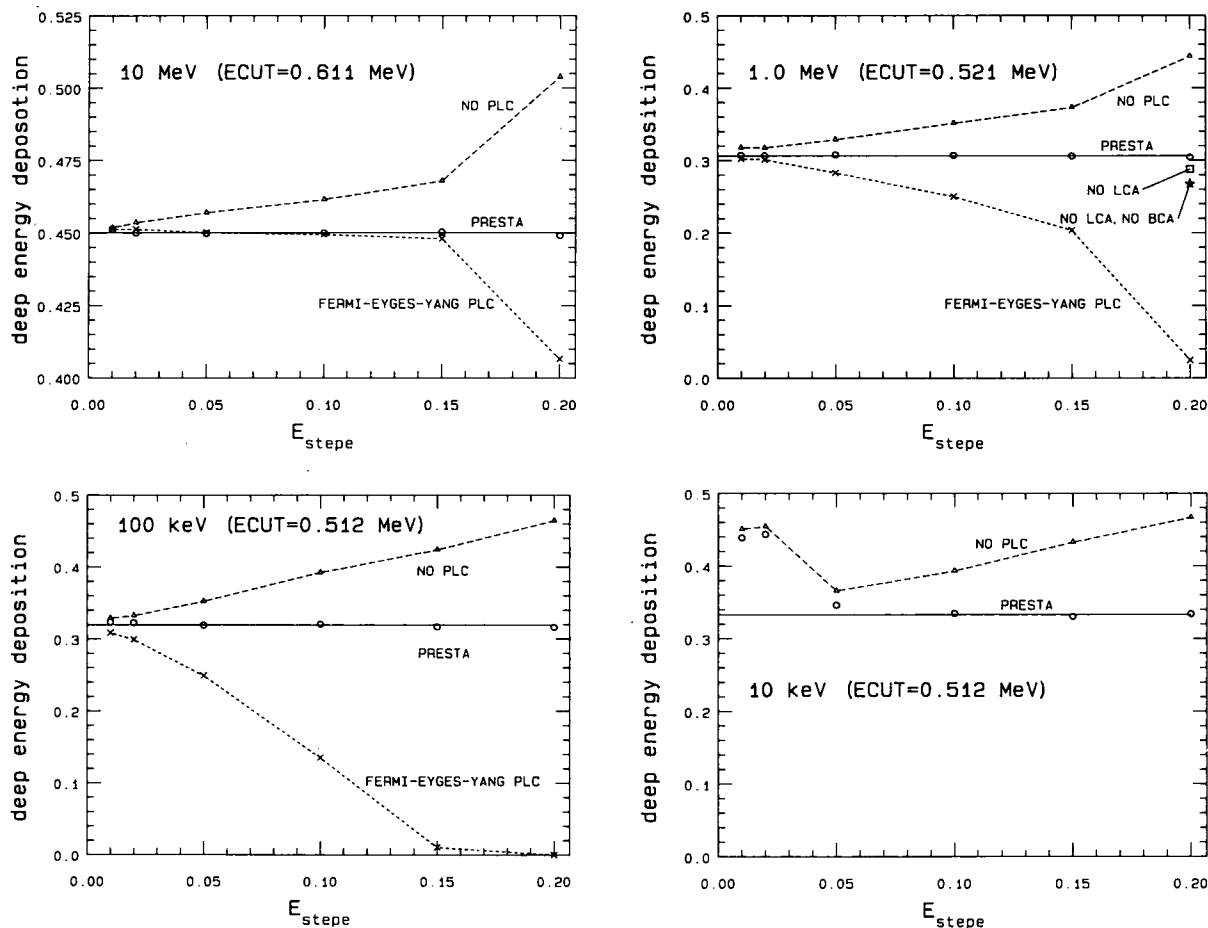


Fig. 11. Fraction of energy deposited past one-half the CSDA range for broad beams of electrons incident on a thick water phantom as a function of the maximum fractional energy loss per step for various electron transport algorithms as labelled. The calculations were done in the CSDA approximation and terminated at the cutoff energies (total) shown. The PRESTA algorithm includes all its components whereas the other algorithms include no LCA or BCA.

plex. If it had been used the LCA would not have affected the values of  $\langle z \rangle$  shown in figs. 7 or 9 but because of an increase in the average straight-line path-length, the width of the  $\langle z \rangle$  distribution would increase. Thus the energy deposited past a certain depth will increase for large depths and decrease for small depths.

### 7.2. Reflection

For this problem the simulations performed were identical to the above cases except that the total amount of energy reflected from the slab was calculated. The results are plotted in fig. 12. Although the PRESTA results are more stable than the results of the simpler algorithms, there still remains dependence on step-size. This is not surprising in view of the fact that PRESTA does not sample straggling distributions about the mean values  $\langle z \rangle$  and  $\langle r \rangle$ . For a particle undergoing a total

curved path  $t$ , if its position were sampled from distributions that allow for straggling, its final position may be anywhere in a sphere of radius  $t$  centered at the particle's initial position. However, from eqs. (2.12) and (3.1) we see that PRESTA only allows the particle to lie within a cone with its vertex at the initial position and aligned along the initial direction of the particle, with height  $s$  and base radius  $\frac{1}{2}t$ . While we have ensured that the average values of longitudinal and lateral displacement are correct, we know that we do not obtain the correct distribution about these averages. The discrepancy is largest in the backwards direction and this is the reason for the step-size dependence in fig. 12. We recognize, however, that the problem we are encountering in this section is one of the most difficult that an electron transport algorithm can be asked to simulate. The lack of straggling distributions represents a shortcoming for PRESTA and indicates the next area for

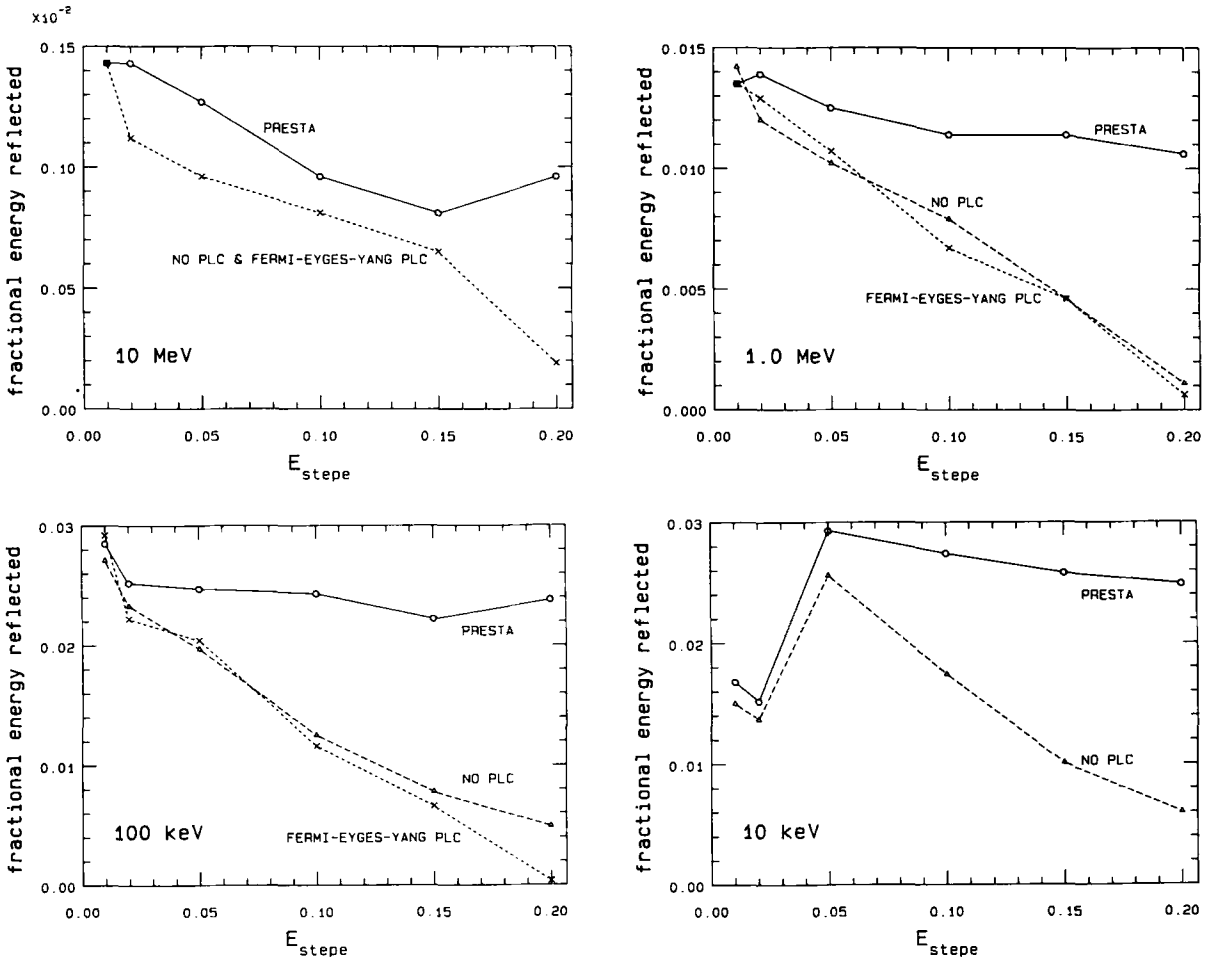


Fig. 12. Fraction of beam energy reflected in the calculations shown in fig. 11.

improvement. At the same time, the reflected component represents a small fraction of the energy involved in most simulations and this is not usually a serious shortcoming.

It is difficult to determine from fig. 12 what the converged values are except that we expect the results for smaller step-sizes to be closer to the truth. Again, the 10 keV case shows evidence of breakdown at small step-sizes.

### 7.3. Ion chamber response

The calculation of the response of thick-walled ion chambers to photon irradiation is a good test for electron transport algorithms because the theory is known [18] and it can predict the response with a high degree of accuracy. Ion chamber response has been the subject of detailed Monte Carlo studies [8,19,20] and it has been found that ion chamber response can be subject to

severe electron step-size dependences.

In fig. 13 we have plotted the response of a thick carbon-walled cylindrical ion chamber (wall thickness 0.273 cm, inner radius 1 cm, inner depth 2 mm) versus  $E_{step}$ , the maximum fractional energy loss per electron step due to "continuous" energy loss processes. The ion chamber was subjected to a broad parallel beam of  $^{60}\text{Co}$  photons, approximated by a monoenergetic "spectrum" of energy 1.25 MeV. The results were normalized to ion chamber theory [18] using correction factors that account for photon attenuation and scatter and electron drift effects that were calculated previously [20]. In fig. 13, all the points at  $E_{step} = 0.2$  and above were calculated using the default step-size,  $t = t_{max}$  for PRESTA and  $t = 0.8 t_{max}$  for EGS.

The curve labelled EGS (delta) was published previously [8] and used the Fermi-Eyges-Yang PLC allowing  $\delta$ -ray and bremsstrahlung photon creation above 10 keV thresholds. The transport cut-offs were set at 10

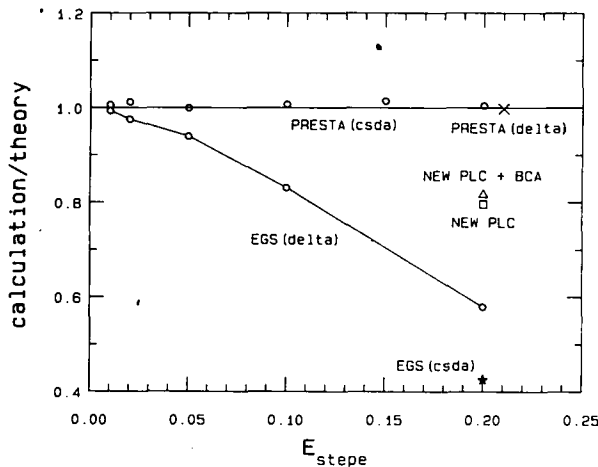


Fig. 13. Response of a carbon-walled pancake ion chamber ( $0.5\text{g cm}^{-2}$  walls, 2 mm deep, 1 cm radius) to  $^{60}\text{Co}$  divided by theory versus ESTEPE for a variety of electron transport algorithms. PRESTA(csda): CSDA calculation using PRESTA; PRESTA(delta): calculation allowing for secondary particle production and transport; EGS(csda): CSDA calculation using current EGS code modified to give a CSDA calculation; EGS(delta): as above but with secondary particle creation and transport; NEW PLC: calculation using the new PLC (no LCA, no BCA); NEW PLC+BCA: calculation using the new PLC and the BCA (no LCA).

keV as well. There is a significant step-size dependence in this curve, as much as 40% for the largest step-size. We also show a similar calculation at the largest step-size for EGS where  $\delta$ -rays and bremsstrahlung photons were not included in the simulation. The effect of  $\delta$ -ray production was incorporated into the stopping powers (EGS(csda), star symbol) and the radiative contribution was ignored with little error. The difference between this and the EGS (delta) case reflects the shortening of effective step-size due to the sampling of discrete electron and bremsstrahlung interactions. The result using the new PLC described in section 2 is shown for the largest step-size (NEW PLC, square symbol). This also is a CSDA calculation and the improvement over the EGS (csda) case is entirely due to the new PLC. Including the BCA offers only minor improvement (NEW PLC + BCA, triangle symbol). Finally, including the LCA gives the results labelled PRESTA for which the agreement at all step-sizes is excellent. We have also calculated the PRESTA result allowing for  $\delta$ -ray creation and transport (PRESTA (delta),  $\times$  symbol). Again it is in excellent agreement with the theory.

This calculation provides an excellent example of the saving in computing time that can be achieved by PRESTA. The PRESTA (delta) calculation executed  $5\frac{1}{2}$  times faster than the EGS (delta,  $E_{\text{step}} = 0.01$ ) calculation which produced results of similar quality. Despite

the overhead of the BCA which is necessary for full implementation of the LCA, much of the electron transport in this calculation takes place far away from any boundaries so that relatively large step-sizes can be permitted and a corresponding gain in computing time is realized.

#### 7.4. Depth-dose curves

Depth-dose curves for broad parallel beams of 100 keV, 1 MeV and 10 MeV electrons on water are shown

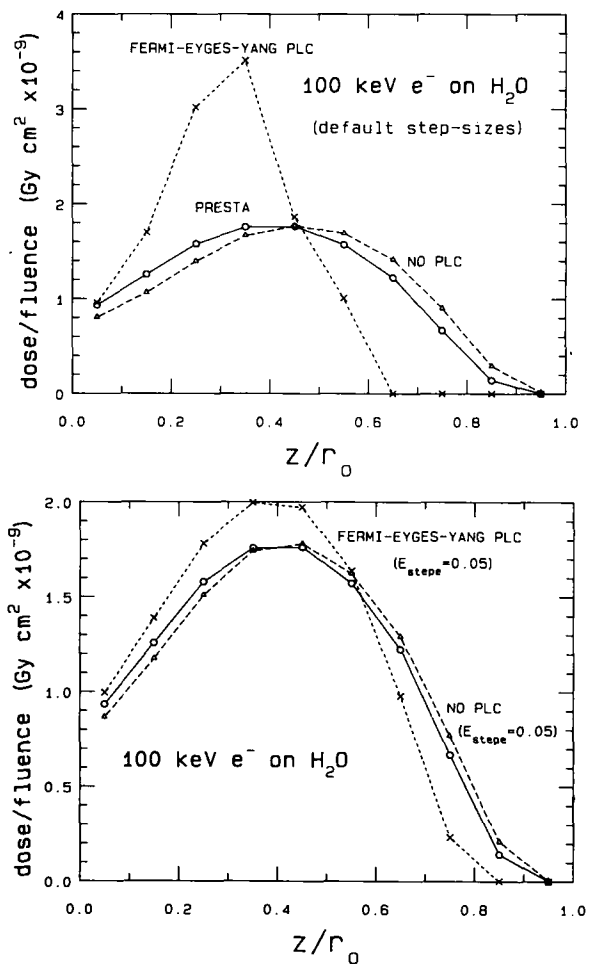


Fig. 14. Depth-dose curves for broad parallel beams of 100 keV electrons incident on a slab of water. Calculations were done in the CSDA approximation with various electron transport algorithms. PRESTA as described here; the Fermi-Eyges-Yang PLC as implemented in the standard EGS; and an EGS calculation with no PLC used. Electrons were followed down to 1% of the incident beam's kinetic energy. Depth is scaled to the CSDA range,  $r_0$ . In the upper figure, the default step sizes for each algorithm are used whereas in the lower a 5% energy loss per step is used for the non-PRESTA algorithms.

in figs. 14 through 16 with the depth normalized to the CSDA range of the incident electrons,  $r_0$ . We show the PRESTA results (circles, solid lines) as well as the EGS results using the Fermi-Eyges-Yang PLC (x's, small dashed curve) and no PLC (triangles, large dashed curve). These were CSDA calculations with secondary particle production accounted for by the use of unrestricted collision stopping powers. The radiative contribution was ignored with little error. In all cases the electrons were transported until they reached a kinetic energy of 1% of the initial kinetic energy whereupon the

remaining energy was deposited "on the spot". The geometry consisted of slabs of thickness  $r_0/10$ .

In the upper half of fig. 14 we show the 100 keV case calculated using default step sizes,  $t = t_{max}$  for PRESTA and  $0.8 t_{max}$  for the others. The qualitative features of the results using the other algorithms may have been anticipated knowing that they lack a proper PLC or BCA. For the Fermi-Eyges-Yang PLC case these compensate for each other at the surface but the peak dose and dose fall-off are quite different. The NO PLC case exhibits a deeper penetration. We have also compared

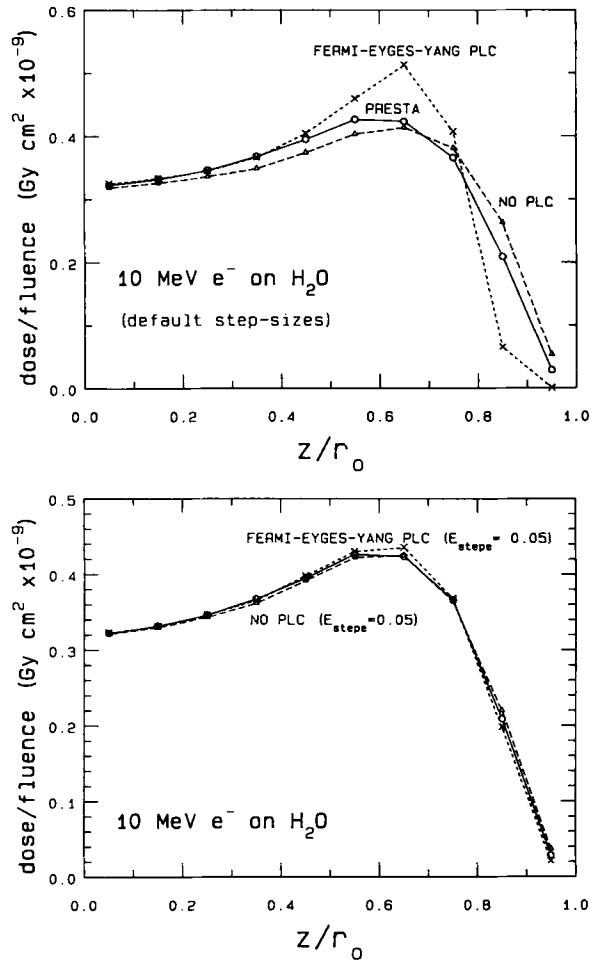
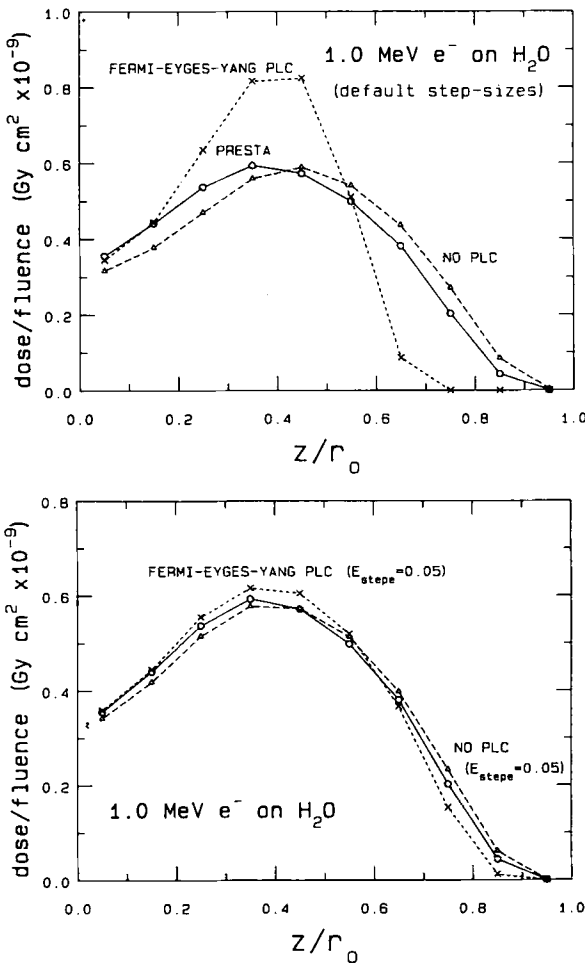


Fig. 15. Depth-dose curves for broad parallel beams of 1 MeV incident electrons on a slab of water. Calculations were done in the CSDA approximation with various electron transport algorithms. PRESTA as described here; the Fermi-Eyges-Yang PLC as implemented in the standard EGS; and an EGS calculation with no PLC used. Electrons were followed down to 1% of the incident beam's kinetic energy. Depth is scaled to the CSDA range,  $r_0$ . In the upper figure, the default step sizes for each algorithm are used whereas in the lower a 5% energy loss per step is used for the non-PRESTA algorithms.

Fig. 16. Depth-dose curves for broad parallel beams of 10 MeV incident electrons on a slab of water. Calculations were done in the CSDA approximation with various electron transport algorithms. PRESTA as described here; the Fermi-Eyges-Yang PLC as implemented in the standard EGS; and an EGS calculation with no PLC used. Electrons were followed down to 1% of the incident beam's kinetic energy. Depth is scaled to the CSDA range,  $r_0$ . In the upper figure, the default step sizes for each algorithm are used whereas in the lower a 5% energy loss per step is used for the non-PRESTA algorithms.

PRESTA using the default step-size versus the other algorithms using  $E_{\text{step}} = 0.05$ . The results are plotted in the lower part of fig. 14 and it is still clear that the other algorithms have not yet converged. (We can assume that PRESTA is step-size independent from the results of section 7.1). In this and all the depth-dose cases it appears that the NO PLC case is closer to the PRESTA result than the Fermi-Eyges-Yang PLC. For step-sizes of the order of 1% the other algorithms converge to the PRESTA result.

For the other energies, 1 MeV in fig. 15 and 10 MeV in fig. 16 the same conclusions can be drawn except that as expected, the other algorithms tend to agree better with PRESTA as the energy increases.

## 8. Computing time comparisons

In this section we compare the computation speed of PRESTA with the standard EGS4 code [11]. We compare 1 and 20 MeV electron depth-dose calculations for depth bin-sizes of  $r_0/10$ ,  $r_0/20$  and  $r_0/40$ . In one set of cases the minimum electron transport energy was set to the energy of an electron that could just cross a depth bin based on its CSDA range. For the 1 MeV case these cutoffs were 0.197, 0.128 and 0.085 MeV for  $r_0/10$ ,  $r_0/20$  and  $r_0/40$  depth bins, respectively. For the 20 MeV case these cutoffs were 1.914, 1.054 and 0.613 MeV. For a second set of calculations the cutoffs were held fixed at 0.010 and 0.189 MeV respectively in order to eliminate differences due to changes in the cutoff. The computations were done on a Vax 11/780 computer with floating-point acceleration. A computer code which allows either PRESTA or the standard EGS4 simulation was used for all calculations. The results for the calculations with variable cutoffs are given in table 1 and 2.

As one decreases the bin size PRESTA takes more

Table 1  
Timing comparison between EGS4 and PRESTA calculations for depth-dose curves with various bin sizes (see text). Variable electron transport cutoffs were used depending on the bin size. For each incident energy, the times are normalized to the PRESTA results for the largest bins.

	$r_0/10$	$r_0/20$	$r_0/40$
<i>1 MeV incident</i>			
PRESTA	(1)	2.2	3.6
EGS4 $E_{\text{step}} = 4\%$	1.7	2.6	3.8
EGS4 $E_{\text{step}} = 1\%$	4.4	6.2	8.6
<i>20 MeV incident</i>			
PRESTA	(1)	2.4	4.3
EGS4 default	1.0	1.5	2.7
EGS4 $E_{\text{step}} = 4\%$	1.9	2.8	4.1
EGS4 $E_{\text{step}} = 1\%$	4.6	6.9	10

Table 2

Timing comparison between EGS4 and PRESTA calculations for depth-dose curves with various bin sizes. Fixed electron transport cutoffs of 0.010 and 0.189 MeV were used at 1 MeV and 20 MeV, respectively. For each incident energy, the times are normalized to the PRESTA results for the largest bins.

	$r_0/10$	$r_0/20$	$r_0/40$
<i>1 MeV incident</i>			
PRESTA	(1)	1.6	2.5
EGS4 $E_{\text{step}} = 4\%$	1.7	1.8	2.1
EGS4 $E_{\text{step}} = 1\%$	4.8	5.4	5.4
<i>20 MeV incident</i>			
PRESTA	(1)	1.7	2.7
EGS4 default	0.44	0.63	1.0
EGS4 $E_{\text{step}} = 4\%$	1.7	1.9	2.1
EGS4 $E_{\text{step}} = 1\%$	5.5	5.7	5.9

computing time due to the increased use of the BCA. However, for a comparable quality of result (see section 7.4), that is,  $E_{\text{step}}$  of 4% or lower for 20 MeV and 1% for 1 MeV, PRESTA is faster by factors as high as 4. The principle saving comes from the more efficient transport of the low energy electrons and the ability of all electrons to take large transport steps when there is no nearby boundary. We have already seen a case in section 7.2 where an ion chamber simulation that involved very few boundaries executed  $5\frac{1}{2}$  times faster using PRESTA than a similar quality calculation using the standard EGS4 methods.

Similar results are obtained if the lower transport threshold is left fixed for the simulation. These results are shown in table 2.

## 9. Conclusion

In this report we have presented PRESTA, a new electron transport algorithm for use in Monte Carlo codes. We have also demonstrated its deployment in the EGS code system although it can be implemented in other codes as well. The new PLC theory may also be used in analytic electron transport calculations. We have not intended to make this report an extensive benchmark of PRESTA against experimentally measured data. This is the ultimate test of any calculation and we leave this for future work and encourage others to do this as well. There is room for improvement in PRESTA and by extensive comparisons with other data the directions for improvement can be clearly indicated.

We believe that PRESTA represents a significant advance in electron transport calculational method. It removes much of the onus on the user to set parameters that govern the electron step-size used in the simulation. By solving many of the problems associated with step-size dependence one is assured that the calculated re-

sults are stable with respect to step-size except in cases where a great deal of backscatter or longitudinal or lateral straggling is involved. This problem has been reduced but not completely eliminated. With PRESTA, the speed of the electron simulation is determined entirely by the secondary particle production thresholds, the lowest energy of transport and the number of boundary crossings. By considering the physics of the simulation a user can simply determine the optimum set of these parameters. Not requiring to establish, for example, the largest  $E_{\text{stepc}}$  that one can "get away with" eliminates much tedious work for the Monte Carlo user and the reliability and credibility of the results are augmented. The savings in computing time can be dramatic, as high as a factor of 6 to obtain the same quality of result when compared to current algorithms. This is made possible by simulating electron paths more accurately and allowing much larger electron step-sizes than previously possible. The additional saving in time because the user does not need to do a detailed study of step-size dependence is more difficult to estimate but it is likely to be substantial.

## References

- [1] S.M. Seltzer and M.J. Berger, Nucl. Instr. and Meth. 119 (1974) 157.
- [2] A.E. Nahum, PhD Thesis, University of Edinburgh (1976) (University Microfilms Int. Order No. 77-7006).
- [3] D.W.O. Rogers, Nucl. Instr. and Meth. A227 (1984) 535.
- [4] P. Andreo and A. Brahme, Radiat. Res. 100 (1984) 16.
- [5] L. Eyges, Phys. Rev. 74 (1948) 1534.
- [6] G.Z. Molière, Z. Naturforsch 2a (1947) 133.
- [7] G.Z. Molière, Z. Naturforsch 3a (1948) 78.
- [8] A.F. Bielajew, D.W.O. Rogers and A.E. Nahum, Phys. Med. Biol. 30 (1985) 419.
- [9] A.F. Bielajew and D.W.O. Rogers, PRESTA - The Parameter Reduced Electron-Step Transport Algorithm for Electron Monte Carlo Transport (NRCC, Ottawa) Report PIRS 0042 (1986).
- [10] R.L. Ford and W.R. Nelson, The EGS code system - Version 3, Stanford Linear Accelerator Center Report SLAC-210 (1978).
- [11] W.R. Nelson, A. Hirayama and D.W.O. Rogers, The EGS4 Code System, Stanford Linear Accelerator Center Report SLAC-265 (Stanford, CA 94305, 1985).
- [12] H.A. Bethe, Phys. Rev. 89 (1953) 1256.
- [13] S. Goudsmit and J.L. Saunderson, Phys. Rev. 57 (1940) 24; Phys. Rev. 58 (1940) 36.
- [14] M.J. Berger and S.M. Seltzer, Stopping Powers and Ranges of Electrons and Positrons, Report NBSIR 82-2250-A (Washington DC: US Dept. of Commerce), (1983).
- [15] H.W. Lewis, Phys. Rev. 78 (1950) 526.
- [16] M.J. Berger Methods in Computational Physics, Vol. 1 (Academic Press, New York, 1963) p. 135.
- [17] C.M. Yang, Phys. Rev. 84 (1951) 599.
- [18] A.F. Bielajew, Phys. Med. Biol. 31 (1986) 161.
- [19] R. Nath and R.J. Schulz, Med. Phys. 8 (1981) 85.
- [20] D.W.O. Rogers, A.F. Bielajew and A.E. Nahum, Phys. Med. Biol. 30 (1985) 429.